Estuaries and Coasts Vol. 30, No. 6, p. 945–958 December 2007

Circulation in Carr Inlet, Puget Sound, During Spring 2003

KATHLEEN A. EDWARDS[1,*], MITSUHIRO KAWASE[2], and CHRISTIAN P. SARASON[3]

[1] *Applied Physics Laboratory, University of Washington, Seattle, Washington 98105-6698*
[2] *School of Oceanography, University of Washington, Seattle, Washington 98105-5351*
[3] *3TIER, 2001 6th Avenue, Suite 2100, Seattle, Washington 98121*

ABSTRACT: The relatively slow flow and exchange of Carr Inlet water with the main basin of Puget Sound, Washington, favor eutrophication. To study Carr Inlet's circulation, the Model-measurement Integration Experiment in Estuary Dynamics (MIXED) was conducted in March–May 2003, spanning the spring bloom. From observations and numerical simulations the circulation was decomposed into tidal and subtidal components; the former was dominated by the M2 tide, the latter by atmospheric forcing. Near the surface, the subtidal velocity was correlated with wind. At mid depths, the subtidal velocity was organized into vertical bands arising from internal waves excited by wind forcing of the water surface. The tidal flow was more strongly steered by local bathymetry and weaker in peak magnitudes than the subtidal flow, yet it contributed more mechanical energy to the inlet. Tidal eddies reduce exchange of water through the inlet's entrances. Numerical simulations with the Princeton Ocean Model recreated many observed features, including the three-layer vertical structure of outflow at the surface and bottom and inflow at mid depth, the mid-depth subtidal response to the wind, and characteristics of the tide. While the model produced greater subtidal flow magnitudes at depth and differences in the phase of the M2 tide compared to observations, overall the case study provided support for more comprehensive simulations of Puget Sound in the future.

Introduction

Puget Sound is a fjord estuary within Washington State on the United States northwest coast. Dominated by the input of the Skagit River and other rivers, the estuarine circulation consists of near-surface outflow of freshwater, compensated by deep salty inflow of Pacific Ocean water. The estuarine circulation supports high productivity because the deep inflow is enriched by nutrients due to upwelling off the Washington coast. In the estuary deep nutrients are mixed upward by shear between the layers, tidal mixing, turbulent flow through constrictions, and high wind stress during storms (Winter et al. 1974; Mackas and Harrison 1997). These processes help make Puget Sound one of the world's most productive salt water environments (Strickland 1983).

The estuarine circulation of the sound is complicated by its bathymetry, which branches into several inlets in the south. Compared to the main basin, flow in the southern inlets is more sluggish and stratified, resulting in lower annual productivity despite an earlier bloom (Strickland 1983). The focus here is the tidal and wind-driven circulation in one of the inlets, Carr Inlet. Its weak circulation and relatively shallow depth increases its vulnerability to eutrophication, a process where nutrient enrichment and accelerated plankton growth leads to reduced oxygen levels (Mackas and Harrison 1997; Washington Department of Ecology 2002, 2003). Carr Inlet is highly sensitive to eutrophication (Newton et al. 1998); after the spring bloom, stratified low-oxygen conditions persist until fall, and primary production is nutrient limited (Bos et al. 2001). Although links between nutrient loading and harmful algal blooms in the inlets are not yet established, Carr Inlet was the site of an outbreak of paralytic shellfish poisoning in August 2000 (Washington Dept. of Ecology 2003). In addition to eutrophication, the inlet's retentive circulation may be important for favoring population differences, as is the case on a larger spatial scale for Puget Sound versus the Juan de Fuca Strait (Rynearson and Armbrust 2004). The inlet's circulation may explain rapid chemical and biological changes observed from mooring data in southern Puget Sound (Dunne et al. 2002; Ruef et al. 2003); the changes may also be due to local biological variability (Emerson personal communication).

The circulation of Carr Inlet (Fig. 1) was studied from observations and numerical simulations made during the Model-measurement Integration eXperiment in Estuary Dynamics (MIXED). Spanning the spring bloom of 2003, MIXED was motivated to improve knowledge of the inlet's dynamics as well as to validate a numerical model, which will be used for future operational simulations of Puget Sound through comparison to field observations.

* Corresponding author; tele: 206-616-4097; fax: 206-543-6785; e-mail: edwards@apl.washington.edu

Methods

FIELD OBSERVATIONS

The mooring and ship observations of Carr Inlet for MIXED were collected during March–April 2003. This time period included a change from

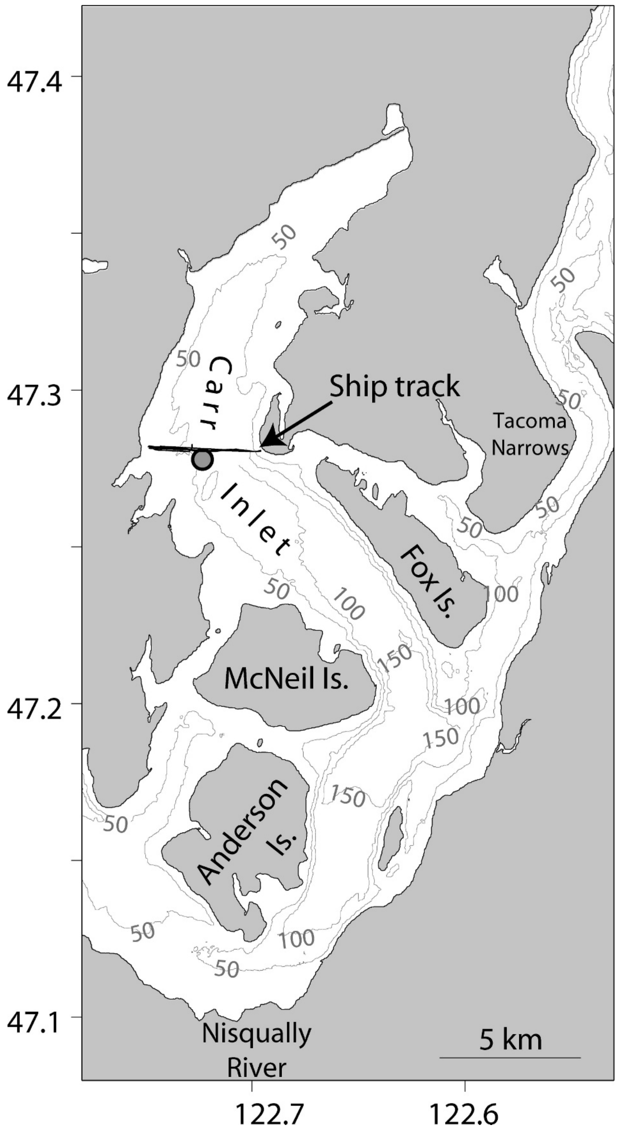

Fig. 1. Study region: Carr Inlet in south Puget Sound, Washington State. Oceanic Remote Chemical/optical Analyzer (ORCA) mooring is located at the large dot; ADCP shiptrack runs east-west through the mooring location (heavy line). Bathymetry is contoured in grey at 50-m increments.

Pacific Standard Time (PST) to Pacific Daylight Time; for consistency, PST is used throughout. Observations collected by other instruments during MIXED, including the Lagrangian BioFloat (D'Asaro 2003; Rehm 2006), CTD casts, and an acoustic rain gauge (Nystuen 2001), are presented elsewhere.

ORCA

The Oceanic Remote Chemical-optical Analyzer (ORCA) is an autonomous moored profiler, which has been placed in different locations in Puget Sound (Dunne et al. 2002; Ruef et al. 2003). At the surface, a float supports a platform carrying a meteorological package and a cell phone to transmit data in real time. Oceanographic convention will be used here for wind direction, which was primarily towards the northeast during MIXED. When along-inlet winds are presented, they have been rotated into the principal axes, which for ORCA are oriented 22° counterclockwise from due east during the MIXED time period. ORCA was moored in Carr Inlet at 47.28 N, 122.72 W from May 2000 to June 2003 at 40 m depth (Fig. 1). During that time ORCA collected profiles of temperature, salinity, oxygen, and chlorophyll. For the MIXED project, ORCA profiled to 20 m depth at 2-h intervals, with deeper profiles to 40 m recorded at noon and midnight.

Shipboard ADCP

To map velocity over the tidal cycle, repeat ship transects were performed across Carr Inlet on April 29, 2003. The ship carried a downward-pointing (Rowe Deines Instruments, RDI) Broadband 300-kHz Acoustic Doppler Current Profiler (ADCP) to collect velocity profiles. Recorded in the instrument's frame of reference, the components of velocity were converted into Earth coordinates during post-processing, during which they were also corrected for the ship's pitch and roll. The profiles were collected in 2-m bins over a 3.2–157.2-m depth range. A profile was collected every 1.4 s as the ship surveyed, producing a median spatial resolution of 113 m in the horizontal. Within 13% of the bottom, the data were contaminated by sidelobe reflection and later discarded. Because of the mounting depth and blanking distance of the ADCP, data above 3.2 m were not recorded.

The cross-inlet transects were performed by the R/V *Skookum* along an east–west line at the 47.28 N of the ORCA mooring (Fig. 1). The shipboard velocity sections were not rotated into along-inlet and cross-inlet coordinates because the local channel direction was hard to define due to the bend in Carr Inlet's alignment; Cartesian coordinates are used instead. The goal of the repeat transects was to resolve the flow over one tidal cycle, although the transition from high to low tide was not captured fully due to personnel limitations.

Errors in ADCP-measured velocity can be introduced through compass misalignment or through incorrect beam orientation, which introduces a scaling error. Estimation of these errors requires auxiliary data such as the ship's velocity (Joyce 1989). Here, continuous measurements of the ship's velocity are lacking due to problems with the ship's Differential Global Positioning System (DGPS). Instead, the ship's velocity is approximated from handheld Global Positioning System (GPS) fixes at the transect ends, i.e., by dividing the cross-transect displacement by the elapsed time. This resembled the transect-averaged ship velocity from bottom-tracking, implying steady ship speed, on several of the transects. Of these, only two transect pairs occurred when the water velocity was relatively constant so that an ensemble average could be performed. Using the transect-averaged water velocity averaged over the upper 20 m, the misalignment angles α were estimated to be 1.30° and 1.24°, corresponding to an error in across-transect velocity of $U_{ship} \sin \alpha = 4$ cm s^{-1} (Joyce et al. 1986), using a typical ship speed of $U_{ship} = 1.9$ m s^{-1}. The scaling factors $(1 + \beta)$ were estimated to be 1.002 and 1.024. With so few error estimates, the correction was not applied, but we note that our conclusions about the layered nature of the flow are unlikely to be altered by the errors. Similarity between the ship velocity estimated from handheld GPS and bottom-tracking during eastward and westward transects suggests that ferromagnetic material on the ship did not strongly affect the ADCP's compass. Without DGPS, the location of the ADCP measurements was obtained by adding the ship's displacement from bottom-tracking to the handheld GPS fix at the start of each transect. The ADCP was bottom-tracking throughout the transects.

Moored ADCP

From March 25 to May 14, 2003, the ORCA mooring was supplemented with a moored ADCP. The ADCP, a downward-pointing RDI 300-kHz broadband, was mounted near the water surface to collect velocity profiles within 2-m vertical bins. The profiles covered 9.0–47.4 m of depth and were averaged in time to 6-min temporal resolution. Before deployment, the ADCP's compass was calibrated by spinning it on a flat nonferrous surface at different angles, as described in the instrument's user guide (RDI 2005). After data collection, the velocity profiles were rotated into along-inlet and cross-inlet coordinates using the angle of the principal axes from the depth-averaged velocity; the angle of rotation was −78° from due east. The rotation could be performed because the velocity at the ORCA location is polarized along the local bathymetry, unlike the cross-inlet velocity sections from the ship to which no single rotation angle applied.

Harmonic tidal analysis was performed on the velocity time series using the t-tide Matlab package (Pawlowicz et al. 2002), which verifies whether the identified tidal constituents are significant based on confidence intervals. The tidal velocity was determined by fitting the significant tidal constituents to the ADCP time series. The subtidal component was obtained by lowpass filtering the time series with the PL64 filter, which removes energy at periods shorter than 38 h (Limeburner 1985).

Model

Description

The Princeton Ocean Model (POM; Blumberg and Mellor 1987) simulated the circulation and stratification of Puget Sound during the MIXED time period. The model equations are those of the standard primitive equation (hydrostatic) dynamics. Given initial and boundary conditions, the model predicts sea-surface elevation, three components of velocity, temperature, salinity, turbulent kinetic energy, and turbulent mixing length. The latter two quantities are used to parameterize vertical mixing by eddies in terms of the turbulence closure scheme of Mellor and Yamada (1974). Surface elevation and depth-averaged velocities are integrated separately from internal quantities in a split-explicit formulation.

The model setup was developed to address overall circulation in Puget Sound (Kawase 1998) and was not tuned for Carr Inlet specifically. A comparison of the model with the MIXED observations in Carr Inlet is used here to benchmark the model's performance. The model domain covers the entire Puget Sound from Admiralty Inlet inwards, as well as a part of the Strait of Juan de Fuca, at a 360-m resolution in the east–west direction and 540-m resolution in the north–south direction. In Carr Inlet this resolution is near the minimum needed to capture flow through the channels bounded by Fox and McNeil Islands. Model bathymetry is derived from data gridded at 30-m horizontal resolution (Finlayson et al. 2000).

The model's surface boundary conditions are the turbulent fluxes of momentum, heat, and freshwater, as well as radiative fluxes. All are derived from the output of the Penn State University-National Center for Atmospheric Research mesoscale atmospheric model, known as MM5. The MM5 output was provided by the University of Washington Department of Atmospheric Sciences (Mass et al. 2003); coupling it to POM is a result of the Puget Sound Regional Synthesis Model (PRISM) program. Oceanographic convention will be used for wind direction. The along-inlet component has been rotated into the principal axes of POM winds, which are oriented 56° counterclockwise from due east, or further to the north than the ORCA winds (22°). The difference in principal axes angle is attributed to steering by local topography that is unresolved by the 4-km MM5 model grid. Averaged over the MIXED time period, the magnitude of MM5 and ORCA winds is similar at 2.6 and 2.3 m s^{-1}, respectively, though the MM5 wind fluctuations are larger, with a standard deviation of 3.3 versus 2.3 m s^{-1} for the daily-averaged winds. To force the oceanographic POM model, turbulent fluxes are derived from MM5 air temperature, humidity, and wind speed using a bulk flux algorithm (Appendix C of Mellor 2003), while the radiative fluxes are output directly from MM5. A no-flux boundary condition is applied at the bottom for mass, heat, and salt, while bottom stress is obtained from a quadratic drag law.

The model has an open boundary in the Strait of Juan de Fuca, where tidal forcing is incorporated as boundary conditions using the scheme of Flather (1976). Seven tidal constituents (M2, K1, S2, N2, O1, P1, and M4) are used, emulating an earlier channel model of Puget Sound tides (Lavelle et al. 1988). A radiation boundary condition is applied to external and internal modes of velocity, while temperature and salinity are either advected out of the model domain or set to a prescribed value when advected in. At the northern edge of the domain, boundary conditions come from climatology of cruise data from the Joint Effort to Monitor the Straits, a partnership led by the Washington State Department of Ecology and PRISM (Newton et al. 2003). Within the domain, river inputs are specified as mass and freshwater sources at the grid points nearest to the mouths of major rivers, using U.S. Geological Survey stream gauge data. Inputs from nongauged streams were extrapolated following Lincoln and Collias (1975). The small tributaries into Carr Inlet (Huge, Minter, Burley, and Purdy creeks) are not included; freshwater also can advect through the inlet's mouth because the much larger Nisqually River discharges nearby (Fig. 1). Freshwater input to the water surface from precipitation is not included, but is expected to be small when compared to the river input of freshwater into the Puget Sound Basin.

Comparison to Observations

The MIXED model run began in December 2002 with initial conditions based on hydrographic data collected by the Washington Department of Ecology, Washington Department of Natural Resources, and PRISM. Model adjustment was complete by the start of the MIXED time period.

The POM velocity time series were compared to the ADCP time series from the MIXED mooring and the shipboard survey. For comparison to the moored data, the POM velocity at the grid point closest to ORCA was rotated into along-inlet and across-inlet coordinates using the principal axes of the depth-averaged POM velocity (-65° from due east). The rotation is possible because the velocity at the grid point is polarized to the local bathymetry. For comparison to the shipboard velocity sections, the POM velocity field was not rotated since the shiptrack cuts across a channel bend and no single rotation angle applies. The tidal analysis described for the moored ADCP velocity was repeated for the POM velocity at the grid point nearest ORCA. Depth-averaging of POM velocity was performed over the 9.4–43.4-m range of the moored ADCP so that the two could be compared directly.

Results

Time Variability

The dominant time variability of circulation in Carr Inlet can be identified in spectra of velocity (Fig. 2) from the moored ADCP and from POM at the grid point nearest ORCA, both based on the 50-day time period from March 25 to May 14, 2003. At all depths, the along-inlet energy is greater than the across-inlet energy at the tidal frequencies, as well as a broad peak at 2–10 d, which spans the multiday weather band and weakens with increasing water depth. Greater along-inlet energy is attributed to bathymetric steering of the flow forced by both the tides and the atmosphere. The POM spectra shapes are similar to those from the ADCP but have a stronger M2 peak at 9.4 m, a stronger K1 peak at 43.4 m, and a stronger weather band peak in the along-inlet spectra at 43.4 m. The ADCP spectra flatten into white noise above 12.1 (cycles per day, cpd), while POM spectra drop off above 7.7 cpd because the model does not resolve the near-turbulent scales measured by the ADCP.

The ADCP vertical coverage misses the near-surface (1.4 m), while the ADCP spectra from deeper depths are similar to one another. POM does resolve the near-surface; its spectrum differs from those for deeper depths. At 1.4 m the cross-inlet weather band peak is stronger than the along-inlet. This is a signature of wind forcing, since the prevalent wind direction near ORCA points more in the across-inlet than along-inlet direction. The vector correlation of POM near-surface velocity and the wind from MM5 has a magnitude of 0.4, significant at the 95% confidence level. This correlation remains significant to ca. 5 m below the surface, though it weakens with depth, indicating that direct wind influence is limited to the near-surface.

Tidal Component of Flow

Depth-averaged Velocity

Tidal analysis of the ADCP depth-averaged velocity shows that the three largest semidiurnal components are M2 (2.7 cm s^{-1} amplitude), S2 (0.9 cm s^{-1}), and N2 (0.7 cm s^{-1}), while the three largest diurnal frequencies are K1 (1.0 cm s^{-1}), O1

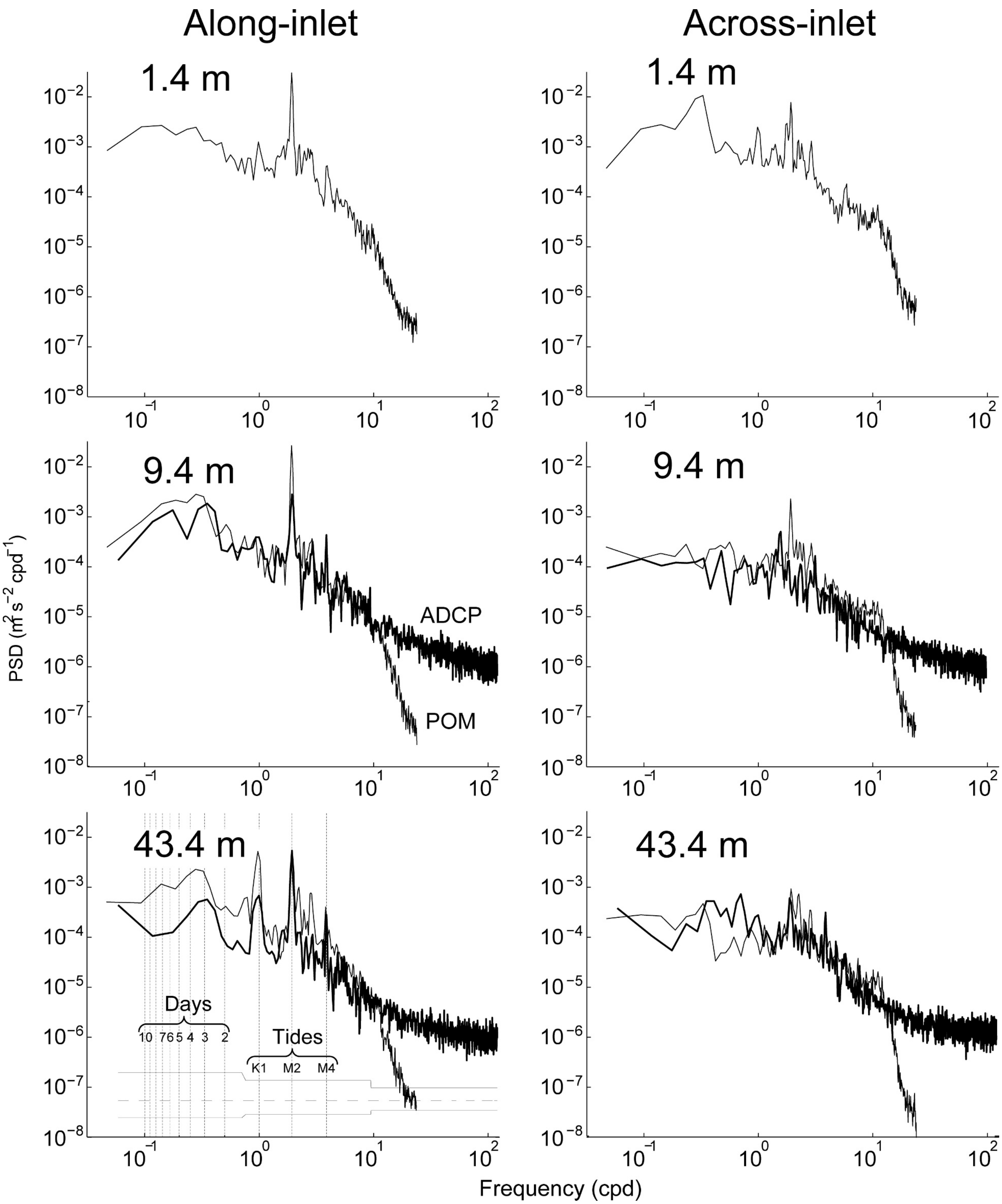

Fig. 2. Spectra of along-inlet and across-inlet velocity at different depths from the moored ADCP (heavy line) and the numerical model at the closest grid point to the ADCP location (light line). No ADCP data available at 1.4 m. The 95% confidence interval (horizontal lines) in lower panel applies to all subplots; tidal constituents and days are labeled.

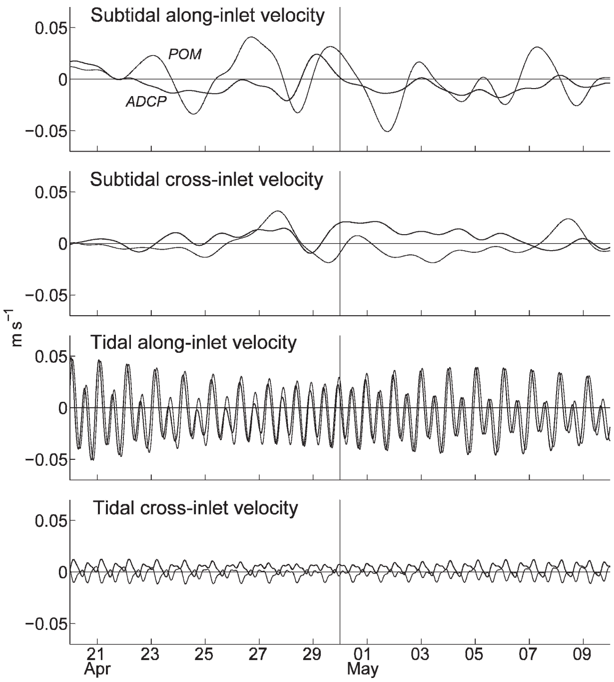

Fig. 3. Depth-averaged velocity time series from moored ADCP (heavy line) and numerical model (light line) for a 20-d period centered on the date of the ship survey (vertical line.

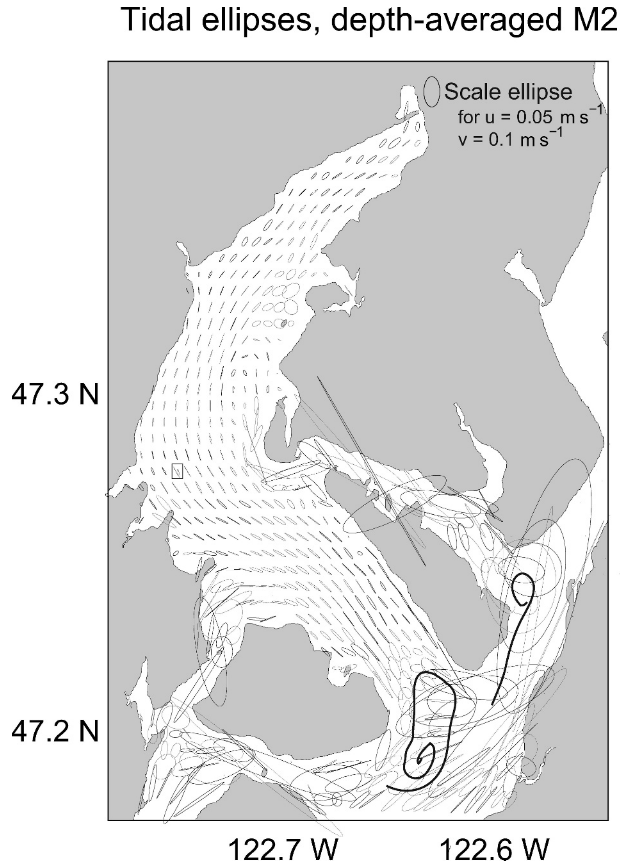

Fig. 4. M2 tidal ellipses for depth-averaged velocity simulated by the numerical model. For visibility, only a few ellipses are plotted where tidal magnitudes become large (outside the inlet mouth and in the passage east of Fox Island). ORCA location is boxed. Scale (upper right) shows an ellipse of $(u, v) = (0.05, 0.1)$ m s^{-1}. Eddies in the tidal velocity field are identified from circular streamlines, such as the low tide examples drawn in heavy lines. Similar eddies are present at the inlet entrances for most of the tidal cycle.

(0.6 cm s^{-1}), and 2Q1 (0.3 cm s^{-1}). Though less energetic, many tidal harmonics are significant at the 95% confidence level; the largest are M03 (0.2 cm s^{-1}) and M4 (0.2 cm s^{-1}). Though POM is forced with fewer tidal harmonics than resolved by the ADCP time series, the amplitudes of major components are similar. The significant semidiurnal components are M2 (2.7 cm s^{-1}) and S2 (0.5 cm s^{-1}), and the largest diurnal components are K1 (0.8 cm s^{-1}) and O1 (0.8 cm s^{-1}). M4 is the largest (0.3 cm s^{-1}) significant shallow water tidal harmonic. The phases of the S2, O1, and K1 components from POM are not statistically different from the ADCP phases, but the M2 phase differs by about 50° (ca. 1.7 h). The phase difference in velocity appears to be larger than that of elevation. At the POM grid cell nearest a tide gauge in Tacoma, 20 km east of Carr Inlet, the phase difference for elevation is 11°. Gauge data were obtained from National Oceanic and Atmospheric Administration's Center for Operational Oceanographic Products and Services.

In the along-inlet direction, peak tidal velocities are similar in magnitude to those of the subtidal velocity, while in the cross-inlet direction, peak tidal velocities are weaker than subtidal velocities (Fig. 3). Both the ADCP and POM along-inlet tidal velocities compare well to the tidal prediction (not shown) of Lavelle et al. (1988), which is averaged over a cross-inlet section through the ORCA location, rather than the point measurements at the ORCA location presented here. Both the ADCP and POM tidal velocity values have similar variations in amplitude and timing of the maxima over the fortnightly tidal cycle, while individual peaks are offset by the 1.7-h phase difference.

Tidal velocities for the cross-inlet depth-averaged flow are weaker than 0.01 m s^{-1}, because the tidal ellipse is narrow and polarized by the local bathymetry (Fig. 4). Comparing POM simulations to the ADCP observations, the velocity maxima (Fig. 3) are concurrent but the cross-inlet flow direction is opposite, so that the rotation around the tidal ellipse is reversed. The narrow ellipses are strongly aligned with the local bathymetry (Fig. 4), which influences the direction of rotation; along the northwest wall of the inlet, rotation in POM is primarily counterclockwise, while along the northeast wall it is clockwise. The sensitivity of the ellipse rotation to local topography may explain why the rotation is opposite at the POM grid cell nearest ORCA; the rotation reverses one grid cell to the west. The central conclusion of Fig. 4, namely that the tidal flow is aligned with bathymetry, is not expected to be affected by the offset shown in Fig. 3, nor by the difference in phase of the M2 tide between POM and ORCA mentioned previously. The tidal velocity in the central part of the inlet is 0.1 m s^{-1}, while it is higher through the narrow passages and adjacent main channels (Fig. 4).

When the velocity field forms recurrent eddies over the tidal cycle, the residence time of water in enclosed regions can increase (e.g., Brooks et al. 1999). In maps of depth-averaged tidal velocity from POM, tidal eddies were identified as circular or closed streamlines. The streamlines defining the eddies at the inlet entrances are shown in Fig. 4 (heavy lines) from the tidal velocity field for low tide. Eddies are present at the entrances for most of the tidal cycle and intensify at both high and low tide. Because they reduce flow through the major entrances, the eddies decrease the exchange of water with the rest of Puget Sound. We interpret these eddies as resulting from the interaction of the tidal flow with topographic features, and expect that the phase misfit shown in Fig. 3 should not affect their presence.

Shipboard ADCP Transects

Repeat ship transects of Carr Inlet record the variability of the velocity field in two dimensions. Covering the transition from high to low tide (Fig. 5), six shipboard ADCP velocity sections were collected over a 9-h period at nominal 1.5-h intervals. The ship transects ran east–west across the ORCA latitude.

At low tide (transect 1), the flow is characterized by three layers. Near-surface outflow is to the southwest (negative u and v in blue) while mid-depth inflow is to the northeast (positive u and v in red). Near the bottom, outflow is to the southeast in the ADCP data and to the southwest in POM. The near-surface outflow is stronger in POM than in the ADCP data. During the rising tide (transects 2–3), the northwestward flow intensifies and rises to the surface with the strongest flow on the inlet's eastern side, while the near-bottom layer of southwestward flow thickens. The near-bottom layer slopes to the west in the ADCP data and to the east in the POM results, which shows stronger flow. A near-surface layer persists in POM with flow to the southwest but is thin or absent in the ADCP data. At high tide (transect 4), the northwestward flow is strongest. Its intensification on the inlet's east side could be influenced by rotation. The width of Carr Inlet, 5 km, is slightly larger than the 3-km internal Rossby radius based on the time-averaged stratification for the MIXED period, while the squared ratio of the Ekman and water depths is small $O(10^{-2})$, indicating that rotation is important (Kasai et al. 2000; Winant 2004). As the tide starts to fall (transects 5–6), the near-bottom layer of southeastward flow intensifies along the inlet's east wall and thickens to mid depths. This layer slopes upward more strongly to the east in POM than in the ADCP observations. In the POM results, a near-surface layer of flow to the southwest is deeper than the thin layer seen in the ADCP data.

While a data comparison is not possible due to the short duration of the ADCP surveys, the POM results show outflow to the southeast at the surface and bottom and inflow to the northwest at mid depth. The layers also appear in the time-mean profile of transport through the section (Fig. 5), which is dominated by the tidal contribution. In an estuary of comparable cross section to Carr Inlet, Estuario Reloncaví, a similar three-layer structure is attributed to the combination of tidal reflection at the estuary head and the estuarine exchange flow (Valle-Levinson et al. 2007).

Subtidal Component of Flow

Depth-averaged Velocity

The moored ADCP and POM time series at the grid point nearest ORCA are used to evaluate the depth-averaged subtidal flow. The source of the peaks in subtidal along-inlet velocity (Fig. 3) is not clear because it is only weakly correlated with the local wind. Both POM and the moored ADCP contain major changes in speed and direction but a weaker match is found for the lesser peaks. The magnitude of the vector correlation between the POM and ADCP subtidal depth-averaged velocity is 0.3, significant at the 95% confidence level. For the cross-inlet velocity, the subtidal component exceeds the weak tidal component due to the channeling of the latter by the bathymetry.

Surface Velocity in Carr Inlet

The subtidal velocity field from POM was interpolated to 0.5 m depth and used to derive streamlines. Figure 6 shows streamlines at a model time close to the start of the shipboard survey on April 29, 2003; this picture is typical of the entire model run in that the subtidal surface velocity is strongly aligned with the wind (overlaid vector). The wind direction during the MIXED period was primarily towards the northeast, with a secondary tendency towards the southwest. On time scales up

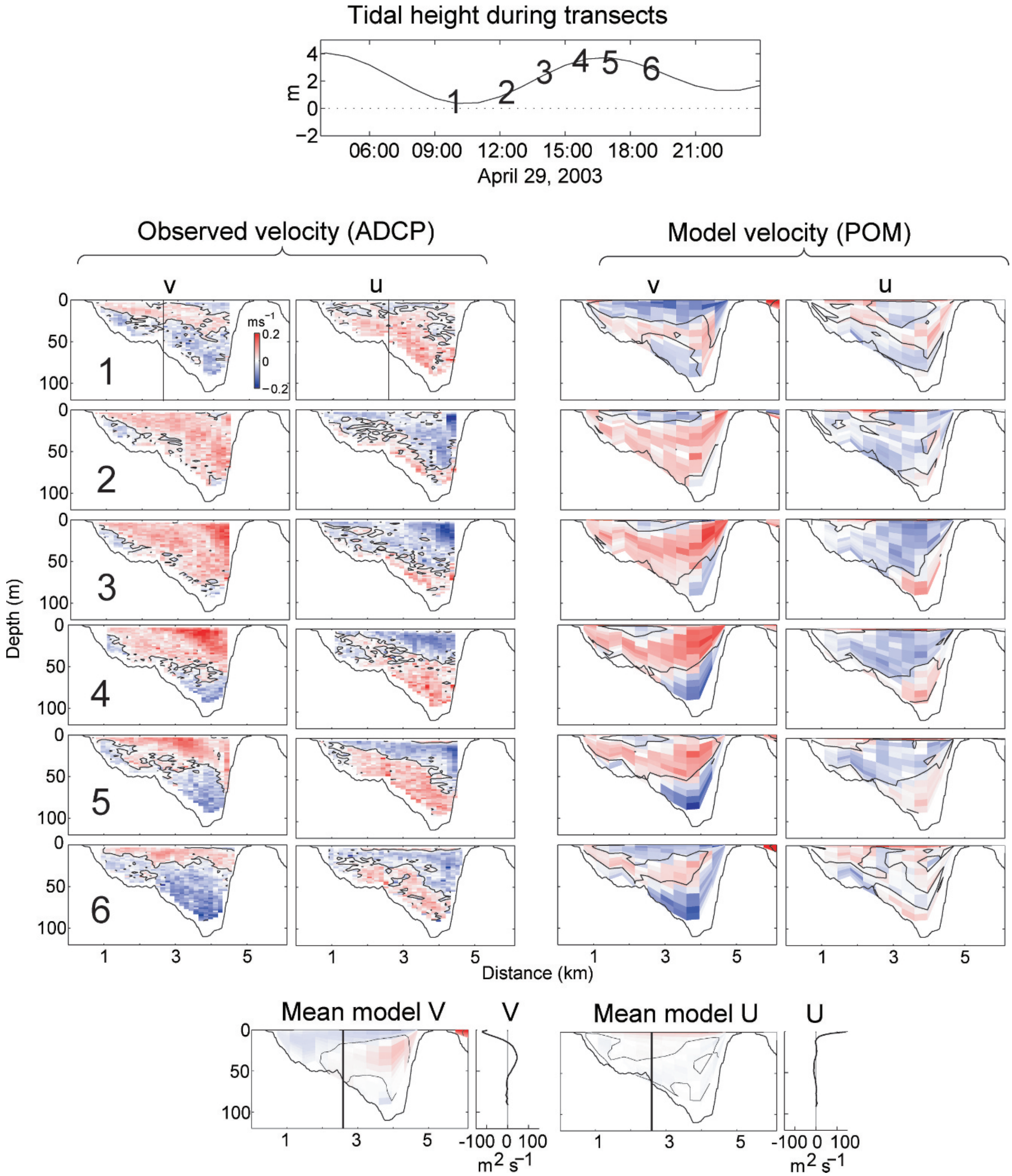

Fig. 5. Over the tidal cycle on April 29, 2003, six vertical sections of v and u velocity from shipboard ADCP (left) and the numerical model (right). Sections obtained along shiptrack in Fig. 1. Light black lines are contours of zero velocity; bottom bathymetry from the ADCP. Color scale and location of ORCA (vertical line) shown in section 1. From the numerical model, time-averaged sections of v and u with profiles of transport integrated across the section. In time-averaged sections of v, northward flow is indicated by a circled cross while southward flow is indicated by a circled dot. For u, eastward and westward flow directions are indicated by vectors; vector is dashed where flow is weak near the bottom.

to the duration of a wind event, the alignment of the subtidal surface velocity with up-inlet wind events could increase surface fluid retention in Carr Inlet. Over longer time scales, the wind-driven contribution is small relative to the time-averaged component, which is directed out of the inlet at the surface. The streamlines in Fig. 6 are for a fixed depth (0.5 m) and so do not include vertical motions at the boundaries where the flow converges. Downwelling occurs along the eastern wall in the time-averaged vertical velocity at 0.5 m from POM.

Horizontal Dispersion

To evaluate the dispersion of surface waters from locations around Carr Inlet, trajectories were calculated using the POM velocity field. The results are shown on trajectory density plots, which indicate the number of trajectories that pass through each model grid cell over a specified time period, here April 1–20, 2003 (Fig. 7). High values of the trajectory density indicate favored paths for advection. At sites around Carr Inlet, 500 simulated parcels were released and advected with the surface velocity field from a single model run. A small random velocity component was added as a token representation of inaccuracies in the simulated advection field. The particles were released over the tidal cycle on the release day in order to avoid tidal biases. Vertical upwelling and downwelling is not permitted, so that the parcels remain at the surface. When a parcel encounters a boundary, it is held there until the simulated velocity field turns back towards model grid cells containing water.

Released at the Inlet head (Fig. 7), the simulated parcels remain near the release site though some spread through the main inlet and out the eastern passages. Releases further south in Carr Inlet (not shown), including at ORCA, are more likely to exit into south Puget Sound and the Tacoma Narrows, especially through the deeper eastern channels. Some of these trajectories also pass north to the inlet head. While the time-averaged transport favors southward flow at the surface (Fig. 5), it is harder for water to enter Carr Inlet from the outside than it is to exit the inlet. Released at the passages between McNeil and Fox Islands, the model trajectories circle the islands but do not enter central Carr Inlet or reach its head. Released at the passage west of Anderson Island, few trajectories enter the inlet through its eastern passages. From the mouth of the Nisqually River, a major freshwater source, most trajectories remain in the main channel, some wrap around the islands, and none enter central Carr Inlet.

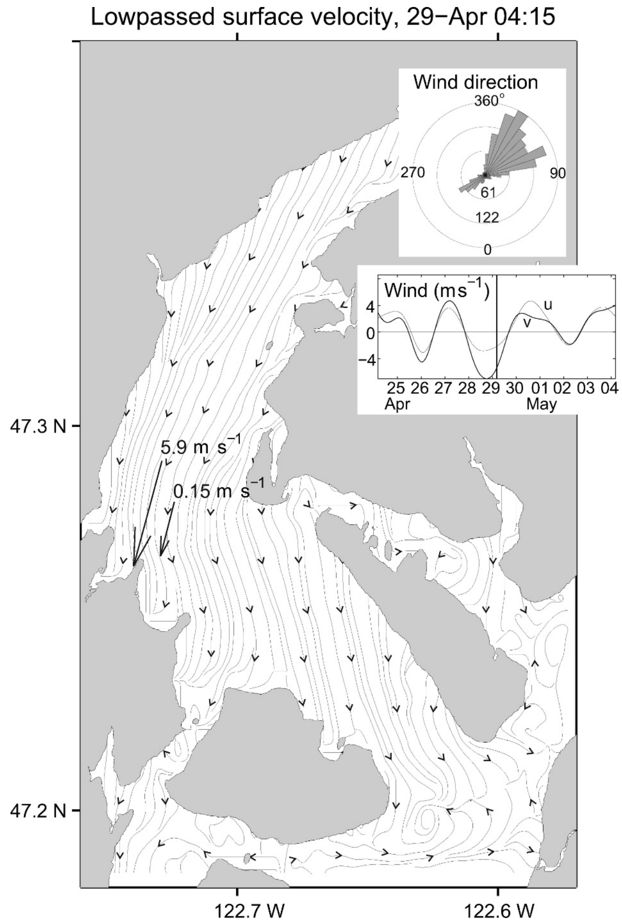

Fig. 6. Streamlines of the subtidal surface velocity on April 29, 2003 at 04:15 GMT, prior to shipboard survey, based on model velocity interpolated to 0.5 m depth. Larger vector is MM5 atmospheric model winds (offset north of mooring location); smaller vector is surface water velocity from the oceanic model at the mooring location (speeds labeled). Histogram of wind direction from atmospheric model for study period (wind direction is in oceanographic convention, so that winds blow primarily towards the northeast). Northward (v) and eastward (u) wind from atmospheric model; vertical line indicates time of map shown in first panel.

Discussion

Internal Wave Analysis

Below the near-surface layer forced directly by the wind, the subtidal velocity appears to be forced indirectly by the wind. Velocity profiles for moored ADCP and POM from the grid point nearest ORCA both show bands of alternating positive and negative flow, though the magnitudes are larger in POM (Fig. 8). The flow reversals appear to fluctuate with the wind, based on the along-inlet component from ORCA's meteorological package and from the MM5 meteorological model used to force POM.

The banding is hypothesized to be the signature of low-frequency wind-excited oscillations in the

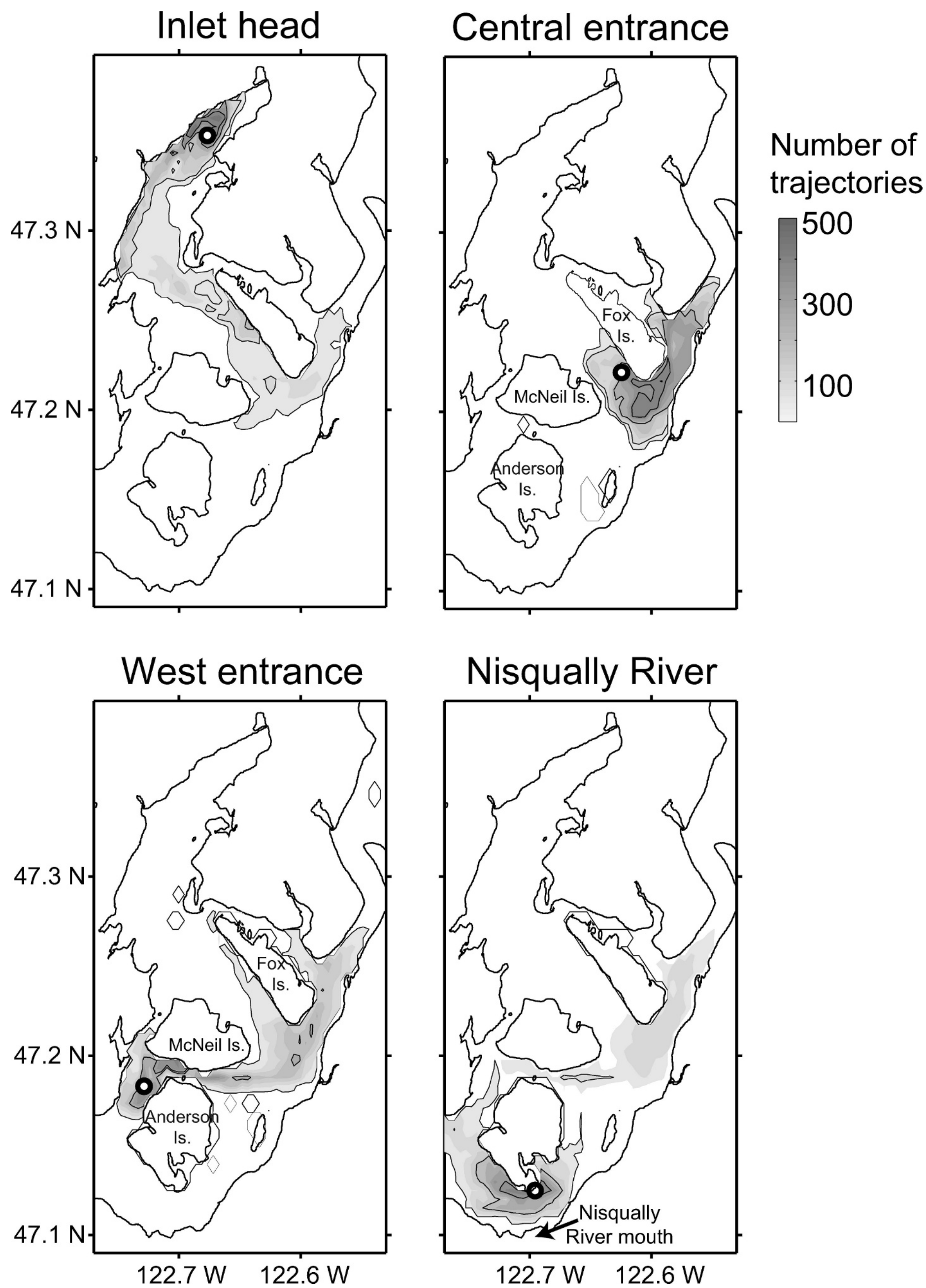

Fig. 7. From the numerical model, trajectory density maps for simulated particles released on April 1, 2003 at locations indicated by the heavy circles: head of Carr Inlet, entrance between McNeill and Fox Islands, Anderson Island entrance, and off the mouth of Nisqually River. Places where the trajectory density is high (dark shading, scale on right) have been visited by the greatest number of parcels over a 19-d period in the model run.

inlet. When the wind blows along a basin, water is pushed against the downwind wall; in compensation for this surface setup, water downwells at the wall and returns upwind at depth. While this process can occur in the absence of stratification (Wong 1994), in the case of a two-layer flow the downwelling at the wall depresses the interface between the layers, and the interface then oscillates. This scenario, developed by Spigel and Imberger (1980), requires sufficient stratification to support the oscillation as well as winds that are of relatively long duration.

To assess whether the wind is persistent enough to establish the oscillation, wind and oscillation time scales are estimated. The wind time scale is approximately 3 d based on the autocorrelation of

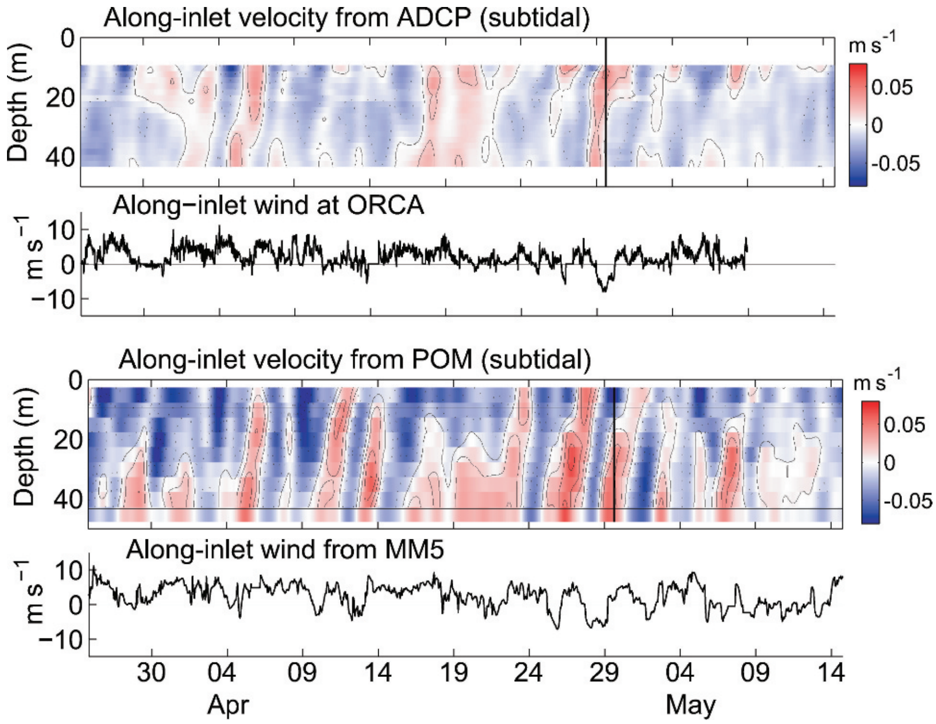

Fig. 8. ADCP subtidal along-inlet velocity with ORCA along-inlet wind (in oceanographic convention). Numerical model subtidal along-inlet velocity with along-inlet wind from atmospheric model at the grid cell nearest ORCA. Vertical line indicates time of ship survey.

wind speed. The oscillation time scale, or the time for an interfacial wave to travel from its generation site at the head of Carr Inlet to ORCA, is derived by considering the two-layer case. During MIXED a shallow upper layer (thickness H_1) overlies a deeper layer (H_2), where the interface depth is based on the depth of relatively stratified water [$\log_{10}(N) > -3.5$] in the ORCA profiles. Using typical values of $g' = 0.0025$ m s^{-2} for reduced gravity and $H_1 = 10$ m and $H_2 = 40$ m for the layer thicknesses, the interfacial wave speed is 0.125 m s^{-1}. At this speed, traveling the 14-km distance from the inlet head to ORCA would require 1.3 d, which is shorter than the 3-d duration of wind forcing. Because the two time scales are close, a moderate change in the density difference between the layers could shut down this mechanism, and indeed the intensity of the banding changes with time.

As an independent test of the wind-excited oscillation hypothesis, the internal wave's horizontal wavelength is compared to the 25-km length of the inlet, L. Order-of-magnitude similarity between the two length scales would support the oscillating interface scenario. The continuously stratified case is now considered because the tilt of the velocity bands is compatible with the upward phase propagation and downward energy propagation of internal waves within a continuously stratified fluid. To obtain the internal wave's horizontal wavelength $\lambda_h = \frac{2\pi}{k}$, the horizontal wave number k is estimated from the dispersion relation $\omega^2 = \frac{N^2 k^2}{k^2 + m^2}$ of internal waves in continuous stratification. The square of the buoyancy frequency $N^2 \sim 9.3037 \times 10^{-5}$ s^{-2} is based on the time-median depth-averaged value from the ORCA profiles, the wave frequency $\omega = \frac{2\pi}{T} \sim 3.2 \times 10^{-5}$ s^{-1} is estimated from the period of $T \sim 2.3$ d of the vertical bands in Fig. 8, and the vertical wave number m is derived from the vertical phase speed $c_{ph_z} = \frac{\omega}{m} \sim 5.2 \times 10^{-4}$ m s^{-1} based on the tilt of the bands in Fig. 8. Using these values, $\lambda_h \sim 31.6$ km, or the same order of magnitude as L although somewhat larger.

These results suggest that it is possible to interpret the vertical banding as a wind-forced oscillation in the inlet. The banding is present throughout the MIXED time period with varying intensity. Similar features have been observed elsewhere; in a continuously-stratified fjord, tilted bands of multiday period were demonstrated by Arneborg and Liljebladh (2001) to be the signature of internal waves generated by energy leaking from pycnocline seiches. A full analysis of whether internal seiches occur in Carr Inlet is beyond the scope of this paper, but we note that the period of the second internal seiche, $T = \frac{4L}{3c_{ph}} = 3.1$ d, is somewhat larger than the spacing of the bands,

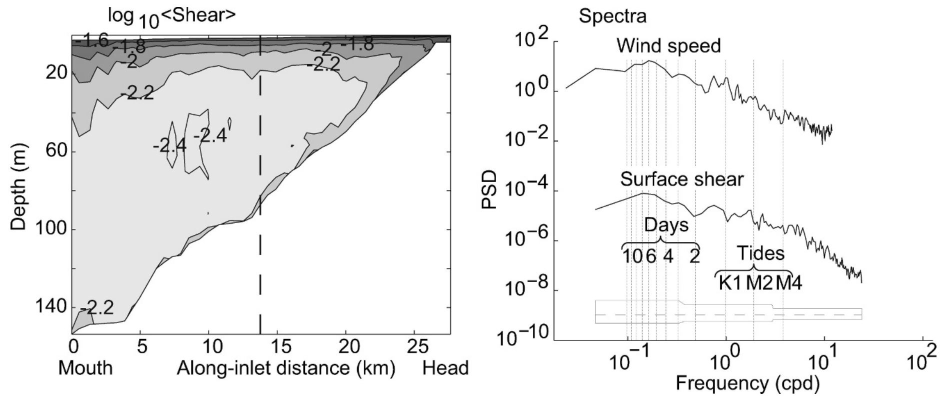

Fig. 9. From the numerical model, time-averaged velocity shear for a vertical section running from the inlet mouth (south) to its head (north) along the deepest part of the inlet; this section runs along the deep eastern side of Carr Inlet. Log of magnitude of time-mean shear is presented. Vertical line is near ORCA location. For the model grid point nearest the mooring, spectra of near-surface velocity shear from the numerical model [s^{-2} cpd^{-1}] and wind speed [m^2 s^{-2} cpd^{-1}] from atmospheric model. The 95% confidence interval is indicated by horizontal lines at the plot bottom; tidal constituents and days are labeled.

using the interfacial wave speed for c_{ph} (Heaps and Ramsbottom 1966).

Shear

The velocity at ORCA can be strongly sheared vertically at a given instant in time (Fig. 5). For Carr Inlet as a whole, locations favorable to mechanical mixing are indicated by high values of velocity shear (Fig. 9). The full Richardson number, which includes the suppression of mixing by buoyancy, is not presented here due to differences between stratification in POM and ORCA. Throughout the inlet, shear is greatest near the water's surface due to processes such as estuarine exchange and wind forcing. The spectra of surface shear and wind speed both have a broad peak in the multiday weather band (Fig. 9).

Relative Importance of Tidal and Wind Forcing in Carr Inlet

The central goal of this study is to better understand the circulation in Carr Inlet. One overall aspect is the relative importance of tidal versus atmospheric forcing on the flow. Initially, this is unclear: in the spectra (Fig. 2), the localized M2 tide is more energetic than the multiday weather band, but during high wind events, the magnitude of the along-inlet subtidal flow is equal to or stronger than the tidal component (Fig. 3). The general assumption in estuaries is that the tides are the dominant source of energy available for mixing (e.g., Officer 1976), but in Carr Inlet the tides are weak with magnitudes of 5 cm s^{-1}, indicating that wind forcing may be more important. Following Kraus and Turner (1967), an upper bound on the mechanical energy input from the wind integrated over the 75-km^2 surface area of Carr Inlet A_s can be estimated as,

$$E_w = \iint \tau v_* \, dt dA_s$$

where the wind stress is $\tau = \rho_a u^2_* = \rho_w v^2_*$, ρ_a is the density of air and ρ_w is the density of sea water. $v_* \sim cu_*$ is the friction velocity for water, where $c = \sqrt{\frac{\rho_a}{\rho_w}}$ is assumed to be a constant value of 0.035 (Farmer 1976), and $u_* = \sqrt{C_{10} U_{10}^2}$ is the friction velocity for air, with the surface drag coefficient $C_{10} \sim 1.2 \times 10^{-3}$ (Large and Pond 1981), and U_{10} is the time series of winds at ORCA adjusted to 10-m measurement height using the algorithm of Fairall et al. (2003). Averaging over the April 2003 time period E_w = 14 kW.

The potential energy input from the barotropic tide is,

$$E_T = \int_H^{\eta} \int_{X_W}^{X_E} p v_T \, dx dz = \int_{X_W}^{X_E} \rho g \eta_T \langle v_T \rangle (\eta_T + H) dx$$

where p is pressure, v_T is the tidal velocity, and the integration is performed horizontally over a west–east section at the latitude of ORCA and vertically from the bottom ($z = H$) to the surface ($z = \eta_T$). The surface displacement due to the dominant M2 tide is η_T, the M2 fit to the velocity is v_T and $<v_T>$ is its depth-average, ρ is the water density, all from POM. The gravitational constant is g. Averaged over April 2003, E_T = 61 kW, which is four times larger than E_w. The tide is more important than the wind in terms of supplying mechanical energy for mixing. In terms of biological response, the tide is less important in Carr Inlet than is weather-band forcing; the latter accounts for more of the variability of chlorophyll and oxygen, as well temperature and salinity (Dunne et al. 2002).

Importance of Carr Inlet to Puget Sound

For the study time period, the importance of Carr Inlet to the larger Puget Sound appears to be weak. Communication of Carr Inlet waters with those of Puget Sound is limited. The horizontal trajectory density analysis (Fig. 7) shows that in central Carr Inlet and towards the head, surface water parcels have difficulty escaping Carr Inlet, while water outside the mouth has limited access to central Carr Inlet. This is due to Carr Inlet's complicated shape, which includes narrow entrances where tidal eddies form (Fig. 4) and decrease exchange with Puget Sound. Such effects can be expected in the other geographically constrained inlets of south Puget Sound. The circulation does not favor a comprehensive seeding of Puget Sound with organisms from Carr Inlet, where spring bloom occurs earlier than in the main basin. The retention and recirculation in the smaller basins of Puget Sound such as Carr Inlet may favor the development of distinct populations, as it does on the larger spatial scales examined by Rynearson and Armbrust (2004).

Acknowledgments

The MIXED project was supported by PRISM, the Applied Physics Laboratory, a University of Washington Royalty Research Grant, and the Washington State Department of Ecology. Kawase and Sarason were also supported by National Oceanographic Partnership Program / Office of Naval Research Grant N00014-02-1-0502. Thanks are extended to participants of MIXED for fieldwork planning, data collection, and discussion: Parker MacCready (moored ADCP); Al Devol, Steve Emerson, and Wendi Ruef (ORCA); Jan Newton and Skip Albertson (R/V *Skookum* data); Eric D'Asaro (BioFloat); and Jeff Nyusten (Acoustic Rain Gauge). Mike Ohmart and Noel Larson collected samples on the cruises, and Kathy Krogslund analyzed the samples. Dale Norton was the captain of the R/V *Skookum*. MM5 output was provided by Cliff Mass and the Olympia wind data were distributed by the University of Washington Department of Atmospheric Sciences. Data from the Joint Effort to Monitor the Straits were provided by Jan Newton.

Literature Cited

Arneborg, L. and B. Liljebladh. 2001. The internal seiches in Gullmar Fjord. Part I: Dynamics. *Journal of Physical Oceanography* 31:2549–2566.

Blumberg, A. F. and G. L. Mellor. 1987. A description of a three-dimensional coastal ocean circulation model, p. 55–88. *In* N. Heaps (ed.), Three-dimensional Coastal Ocean Models, Volume 4. American Geophysical Union, Washington, D.C.

Bos, J. K., R. A. Reynolds, J. Newton, and S. A. Albertson. 2001. Assessing sensitivity to eutrophication of the southern Puget Sound basin: Spatial and seasonal perspectives. Proceedings of the Puget Sound Research Conference, Seattle, Washington.

Brooks, D. A., M. W. Baca, and Y.-T. Lo. 1999. Tidal circulation and residence time in a macrotidal estuary: Cobscook Bay, Maine. *Estuarine, Coastal and Shelf Science* 49:647–665.

D'Asaro, E. A. 2003. Performance of autonomous Lagrangian floats. *Journal of Atmospheric and Oceanic Technology* 20:896–911.

Dunne, J. P., A. H. Devol, and S. Emerson. 2002. The Oceanic Remote Chemical/Optical Analyzer (ORCA): An autonomous moored profiler. *Journal of Atmospheric and Oceanic Technology* 19: 1709–1721.

Fairall, C. W., E. F. Bradley, J. E. Hare, A. A. Grachev, and J. B. Edson. 2003. Bulk parameterization of air–sea fluxes: Updates and verification for the COARE algorithm. *Journal of Climate* 16: 571–591.

Farmer, D. M. 1976. The influence of wind on the surface layer of a stratified inlet: Part II. Analysis. *Journal of Physical Oceanography* 6:941–952.

Finlayson, D. P., R. A. Haugerud, H. Greenberg, and M. G. Logsdon. 2000. Puget Sound Digital Elevation Model. University of Washington, Seattle, Washington. (http://students.washington.edu/dfinlays/pugetsound/).

Flather, R. A. 1976. A tidal model of the northwest European continental shelf. *Memoires de la Society Royal des Sciences de Liege* 10:141–164.

Heaps, N. S. and A. E. Ramsbottom. 1966. Wind effects on the water in a narrow two-layered lake. *Philosophical Transactions for the Royal Society of London* 259:391–430.

Joyce, T. M. 1989. On the in 'situ' calibration' of shipboard ADCP. *Journal of Atmospheric and Oceanic Technology* 6: 169–172.

Joyce, T. M., C. Wunsch, and S. D. Pierce. 1986. Synoptic Gulf Stream velocity profiles through simultaneous inversion of hydrographic and acoustic Doppler data. *Journal of Geophysical Research* 91:7573–7585.

Kasai, A., A. E. Hill, T. Fujiwara, and J. H. Simpson. 2000. Effect of the Earth's rotation on the circulation in regions of freshwater influence. *Journal of Geophysical Research* 105:16,961–16,969.

Kawase, M. 1998. A numerical model of Puget Sound circulation, p. 209–216. *In*Proceedings of the Puget Sound Research Conference, Seattle, Washington.

Kraus, E. B. and J. S. Turner. 1967. A one-dimensional model of the seasonal thermocline. *Tellus* 19:98–105.

Large, W. and S. Pond. 1981. Open ocean momentum flux measurements in moderate to strong winds. *Journal of Physical Oceanography* 11:324–336.

Lavelle, J. W., H. O. Mofjeld, E. Lempriere-Doggett, G. A. Cannon, D. J. Pashinski, E. D. Cokelet, L. Lytle, and S. Gill. 1988. A multiply-connected channel model of tides and tidal currents in Puget Sound, Washington and a comparison with updated observations. National Oceanic and Atmospheric Administration Technical Memo ERL PMEL-84. Seattle, WA.

Limeburner, R. 1985. CODE 2: Moored array and large-scale data report. CODE Technical Report No. 38, Woods Hole Oceanographic Institute Technical Report 85-35. Woods Hole, MA.

Lincoln, J. H. and E. Collias. 1975. An oceanographic study of the Port Orchard system. University of Washington Report for URS, M75-102. Seattle, Washington.

Mackas, D. L. and P. J. Harrison. 1997. Nitrogenous nutrient sources and sinks in the Juan de Fuca Strait/Strait of Georgia/ Puget Sound estuarine system: Assessing the potential for eutrophication. *Estuarine, Coastal and Shelf Science* 44:1–21.

Mass, C. F., M. Albright, D. Ovens, R. Steed, M. MacIver, E. Grimit, T. Eckel, B. Lamb, J. Vaughan, K. Westrick, P. Storck, B. Colman, C. Hill, N. Maykut, M. Gilroy, S. A. Ferguson, J. Yetter, J. M. Sierchio, C. Bowman, R. Stender, R. Wilson, and W. Brown. 2003. Regional environmental prediction over the Pacific Northwest. *Bulletin of the American Meteorological Society* 84: 1353–1366.

Mellor, G. L. 2003. Users guide for a three-dimensional, primitive equation, numerical ocean model, June 2003 version. Progress in Atmospheric and Oceanic Sciences, Princeton University, Princeton, New Jersey.

Mellor, G. L. and T. Yamada. 1974. A hierarchy of turbulence closure models for planetary boundary layers. *Journal of the Atmospheric Sciences* 31:1791–1806.

Newton, J., S. Albertson, and A. Thomson. 1998. Washington state marine water quality in 1996 and 1997. Technical Report 98-338. Washington State Department of Ecology, Olympia, Washington.

Newton, J. A., E. Siegel, and S. L. Albertson. 2003. Oceanographic changes in Puget Sound and the Strait of Juan de Fuca during the 2000-01 drought. *Canadian Water Resources Journal* 28:715–728.

Nystuen, J. A. 2001. Listening to raindrops from underwater: An acoustic disdrometer. *Journal of Atmospheric and Oceanic Technology* 18:1640–1657.

Officer, C. B. 1976. Physical Oceanography of Estuaries (and Associated Coastal Waters). John Wiley and Sons, New York.

Pawlowicz, R., B. Beardsley, and S. Lentz. 2002. Classical tidal harmonic analysis including error estimates in Matlab using T_TIDE. *Computational Geosciences* 28:929–937.

RDI. 2005. WorkHorse Monitor ADCP User's Guide. Teledyne RD Instruments, Poway, California. Available online at www.rdinstruments.com.

Rehm, E. 2006. In-situ measurement of primary productivity from a Lagrangian float. Ocean Sciences Meeting Supplement, Abstract OS25N-10. Eos Transactions, American Geophysical Union 87.

Ruef, W., A. Devol, S. Emerson, J. Dunne, J. Newton, R. Reynolds, and J. Lynton. 2003. In situ and remote monitoring of water quality in south Puget Sound: The ORCA time series. Proceedings of the 2003 Georgia Basin/Puget Sound Research Conference, Vancouver, Canada.

Rynearson, T. A. and E. V. Armbrust. 2004. Genetic differentiation among populations of the planktonic marine diatom *Ditylum brightwellii* (Bacillariophyceae). *Journal of Phycology* 40: 34–43.

Spigel, R. H. and J. Imberger. 1980. The classification of mixed-layer dynamics in lakes of small to medium size. *Journal of Physical Oceanography* 10:1104–1121.

Strickland, R. M. 1983. The Fertile Fjord. Puget Sound Books, Washington Sea Grant Publication, Seattle, Washington.

Valle-Levinson, A., N. Sarkar, R. Sanya, D. Soto, and J. Leon. 2007. Spatial structure of hydrography and flow in a Chilean fjord, Estuario Reloncaví. *Estuaries and Coasts* 30:113–126.

Washington Department of Ecology. 2002. Georgia Basin-Puget Sound Ecosystem Indicators Report, Spring 2002. Technical Report 02-01-002, Washington State Department of Ecology, Olympia, Washington.

Washington Department of Ecology. 2003. South Puget Sound Model Nutrient Study. Washington State Department of Ecology, Olympia, Washington. http://www.ecy.wa.gov/programs/eap/spasm/.

Winant, C. D. 2004. Three-dimensional flow in an elongated, rotating basin. *Journal of Physical Oceanography* 34:462–476.

Winter, D. F., K. Banse, and G. C. Anderson. 1974. The dynamics of phytoplankton blooms in Puget Sound, a fjord in the Northwestern United States. *Marine Biology* 29:139–176.

Wong, K.-C. 1994. On the nature of transverse variability in a coastal plain estuary. *Journal of Geophysical Research* 99:14,209–14,222.

Sources of Unpublished Materials

Devol, A. personal communication. School of Oceanography, Box 357940, University of Washington, Seattle, WA 98195-7940

Emerson, S. personal communication. School of Oceanography, Box 357940, University of Washington, Seattle, WA 98195-7940

Newton, J. personal communication. Applied Physics Laboratory, Box 355640, University of Washington, Seattle, WA 98105-6698

Received, February 6, 2007
Revised, June 25, 2007
Accepted, August 28, 2007